Combining Alginate/PVPI-Based Film with Frequency Rhythmic Electrical Modulation System (FREMS) Technology as an Advanced Strategy for Diabetic Wounds

Marco Contardi,* Maria Summa, Martina Lenzuni, Luigi Miracoli, Franco Bertora, Maurizio Diaz Mendez, Athanassia Athanassiou,* and Rosalia Bertorelli*

Diabetes is rising as one of the most diffused diseases of the century with the related urgent necessity to face its systemic and local effects on the patients, such as cardiovascular problems, degeneration of limbs, and dysfunction of the wound healing process. The diffusion of leg ulcers has been estimated to be 1.51 for 1000 population, and these non-resolved wounds can produce several social, economic, and mental health issues in diabetic patients. At the same time, these people experience neuropathic pain that causes morbidity and a further decrease in their quality of life. Here, a new study is presented where asodium alginate/Polyvinylpyrrolidone-Iodine complex (PVPI)-based wound dressing is combined with the Frequency Rhythmic Electrical Modulation System (FREMS) technology, an established medical device for the treatment of neuropathic pain and diabetic ulcers. The produced Alginate/PVPI-based films are characterized in terms of morphology, chemistry, wettability, bio-/hemo-compatibility, and clotting capacity. Next, the Alginate/PVPI-based films are used together with FREMS technology in diabetic mice models, and synergism of their action in the wound closure rate and anti-inflammatory properties is found. Hence, how the combination of electrical neurostimulation devices and advanced wound dressings can be a new approach to improve chronic wound treatment is demonstrated.

M. Contardi, M. Lenzuni, A. Athanassiou
Smart Materials
Istituto Italiano di Tecnologia
Via Morego 30, Genova 16163, Italy
E-mail: marco.contardi@iit.it; athanassia.athanassiou@iit.it

M. Summa, R. Bertorelli
Translational Pharmacology
Istituto Italiano di Tecnologia
Via Morego 30, Genova 16163, Italy
E-mail: Rosalia.bertorelli@iit.it

L. Miracoli, F. Bertora, M. D. Mendez
Fremslife Srl, R&D Dept.
Via Buccari, 9, Genova 16153, Italy

1. Introduction

Nowadays, diabetes is considered the most critical non-communicable global disease fostered by an unhealthy modern lifestyle.[1] This metabolic disorder characterized by hyperglycemia is a well-declared socioeconomic burden that affects more than 400 million people worldwide.[2] Diabetes's effects deeply compromise patients' functionality, provoking severe neuropathic pain, cardiovascular issues, and, in the late stage, correlated disorders like the onset of Alzheimer's disease.[3] Among diabetic people, one in four will experience a diabetic foot ulcer and correlated problems during their lifetime. The progression of all these factors can lead to the amputation of part of the limb.[4]

Diabetic ulcers occur with a prevalence of 1.51 per 1000 population and this number is predicted to increase with the enhancement of the elderly population worldwide.[4a,5] They are characterized by a chronic inflammatory environment where the healing steps (hemostasis, inflammation, proliferation, and remodeling) are disrupted, causing a prolonged absence of the skin barrier.[6] This scenario is a perfect condition for triggering harmful microorganism infections, which further delay the repair of the wound, increasing the cost of the management and issues for the patients.[6b,7]

Wound dressings have been designed to control and support the healing of ulcers locally, where traditional tools, such as gauze and bandages, fail. Advanced wound dressings were intended in the form of films, fibrous mats, foams, and hydrogels for the in situ delivery of antibiotics, antioxidant and anti-inflammatory molecules, and growth factors.[8] At the same time, these advanced dressings attempt to contrast microorganisms' invasion and proliferation, absorb the exudate, re-equilibrate the persistent inflammatory condition, and promote skin cell proliferation to achieve successful wound repair.[9] In this regard, several natural and synthetic polymers, and even fungal mycelium have been tested in the recent past.[10] Among the proposed biomaterials, alginate-based dressings offer considerable biocompatibility and tissue tolerance, the capacity to enhance cell proliferation, release active compounds, absorb exudate to

maintain proper moisture in the wound bed, and comprehensively ameliorate the condition of diabetic ulcers.[11] Recently, the combination of Alginate and PVPI (Polyvinylpyrrolidone complexed with iodine) as an antiseptic agent showed excellent performance as wound dressing with healing, antimicrobial and anti-inflammatory properties, suggesting that it can be a good candidate for its potential application even at a clinical level.[12] PVPI can ensure an excellent effect against harmful pathogens, such as *Escherichia coli*, *Staphylococcus aureus*, *Pseudomonas aeruginosa*, and *Candida albicans*, that commonly invade unsolved wounds.[12a,13]

Nevertheless, even the advanced wound dressings are not designed to face poor blood flow, peripheral neuropathic pain, and the loss of cutaneous sensibility. These diabetic systemic effects cause intense pain and morbidity, which are considerable problems in the daily life of diabetic patients. The management of neuropathic pain is considered a significant unmet medical need,[14] and the current treatments are based on either pharmacological therapies or invasive and not invasive peripheral stimulation.[15] Electrical stimulation is a non-invasive tool for treating neuropathic pain and enhancing the circulation flow in diabetic patients. This technology has been explored using different electrical stimulation, applied currents (direct, pulsating, alternating), and set-ups.[16] However, transcutaneous electrical nerve stimulation (TENS) and FREMS (Frequency Rhythmic Electrical Modulation System) are the two most studied and applied techniques for this issue.

FREMS technology offers a unique stimulation modality that changes electrical frequencies and amplitudes during the treatment. This stimulation showed positive effects in treating neuropathic pain and the capacity to increase the blood flow where applied, causing an overall improvement in the patient's quality of life.[16–17] Specifically, clinical data collected in previous studies suggest that FREMS treatments improve wound healing and increase pain control compared with conventional medical therapy in patients with chronic leg ulcers of mixed etiology. Actions on endothelial and vascular smooth muscle cells have been highlighted, especially in relation to the effects of synchronous depolarization, vasomotion, and release of Nitric Oxide (NO), which can have an anti-inflammatory action, and modulation of angiogenic growth factors such as the vascular endothelial growth factor (VEGF), that is one of the most potent inducers of vascular permeability, and it is also a potent mitogen of vascular endothelial cells.[18]

However, the FREMS technology does not provide antibacterial or antifungal actions and cannot ensure any covering action of the wound or a proper moisture-wound bed environment.

In this work, we investigate the combination of the FREMS technology with Alginate-PVPI-based wound dressing as a complete solution for diabetic wounds. We first described the wound dressing's production and its morphological and physicochemical features. Then we present the studies on the biocompatibility, hemocompatibility, and clotting properties of Alg-PVPI films, and finally, we demonstrate the combination of Alg-PVPI films with FREMS technology on in vivo full-thickness excisional skin wound healing diabetic mice model for the wound closure rate and the anti-inflammatory properties evaluation.

2. Experimental Section

2.1. Materials

Alginic acid sodium salt (Alg) with a viscosity of 15 000–20 000 cps, PVPI), glycerol (Gly) (density = 1.261 g cm^{-3}), CaCl$_2$ salt, heparin sodium salt, Dulbecco's phosphate buffered saline (PBS), glutaraldehyde, osmium tetroxide, ethanol, and sodium cacodylate buffer were purchased from Sigma-Aldrich (St. Louis, USA) and used as received. Deionized water was obtained from a Milli-Q Advantage A10 ultrapure water purification system (Merck-Millipore, Darmstadt, Germany). HaCaT cells were purchased from Cell Line Service (Heidelberg, Germany), 300 493. CellTiter-Glo reagent was purchased from Promega (Madison, WI). C57BL/6J male mice were purchased from Charles River, Calco, Italy. Gauzes made of cotton were purchased from GIMA S.p.a. (Via Marconi, 1, 20060, Gessato (Mi), Italy).

2.2. Preparation of Films

A slightly different protocol was used with respect to ref. [12a,b,] for the fabrication of Alg-PVPI films. Specifically, 600 mg of Alg, 30 mg PVPI, and 400 mg of Gly were dissolved in 10 mL of MilliQ water. The solution was kept under shaking for 24 h to obtain a homogenous dispersion. Afterward, the viscous solution was transferred inside a syringe, and microscope slides were cut into square shapes of 1.5 × 1.5 cm using a diamond drill. A glass square was blocked on the spin coater system (model WS-650S-6NPP/LITE/OND by Laurell Technologies Corporation, Philadelphia, USA), and 1 mL of the viscous solution was poured into it. The spin coating process was carried out with the following parameters: final speed of 180 rpm, acceleration of 35 rpm, and duration of 90 s. After the spin coating process, the films were dried in the dark under an aspirated hood overnight. Finally, the dried films were gently separated from the glass substrate using a tweezer.

2.3. Morphological Analysis

The morphology of the obtained Alg-PVPI films was analyzed by Scanning Electron Microscopy (SEM), using a variable pressure JEOL JSM-649LA (JEOL, Tokyo, Japan) microscope equipped with a tungsten thermionic electron source and working in high vacuum mode, with an acceleration voltage of 10 kV. The specimens were coated with a 10 nm thick film of gold utilizing a Cressington Sputter Coater–208 HR (Cressington, Watford, UK).

2.4. ATR-FTIR Spectroscopy

Infrared spectra of the Alg-PVPI materials were acquired using an Attenuated Total Reflectance (ATR) accessory (MIRacle ATR, PIKE Technologies) with a diamond crystal coupled to a Fourier Transform Infrared (FTIR) spectrometer (Vertex 70v FT-IR, Bruker). All spectra were recorded between 4000 and 600 cm^{-1}, with a resolution of 4 cm^{-1}, accumulating 128 scans.

**ADVANCED
SCIENCE NEWS**

www.advancedsciencenews.com

**Macro-
molecular
Bioscience**

www.mbs-journal.de

2.5. Water Contact Angle

Water contact angle (WCA) measurements were performed by a contact angle goniometer (OCA-20 DataPhysics, Germany) to evaluate the water wettability of the films. The sessile drop technique was used with 5 µL MilliQ water drops dispensed from a microsyringe. The drops were deposited on random spots, and six measurements were averaged to get a reliable value ($n = 6$).

2.6. Biocompatibility Assay

Human epidermal keratinocyte (HaCaT) cells were cultured in Dulbecco's Modified Eagle Medium (DMEM) supplemented with 10% fetal bovine serum (FBS) and 2 mmol L^{-1} L-glutamine at 37 °C in an atmosphere of 5% CO_2 and 95% air. HaCaT cells were seeded in 96- well plates at a density of 4.0×10^5 in a final medium well volume of 100 µL and incubation until the proper confluence was reached. After 24 h of treatment, cells were rapidly rinsed with pre-warmed phosphate-buffered saline (PBS) with Ca^{2+}/Mg^{2+}, and the extraction medium was re-placed with the medium containing the extract from the Alg-PVPI films (control samples were treated with medium processed as the extractions), and cells were incubated for additional 24 h and 48 h. Extracts were prepared by placing Alg-PVPI films in cell media at the concentrations of 0.5, 1.0, 2.5, and 5.0 mg mL^{-1}. According to ISO10993-5 guidelines, as the cell viability of the samples with extracts was higher than 70% of the control group, all materials were considered biocompatible. Cell viability was determined by measuring ATP levels by CellTiter-Glo assay, as indicated by the supplier as percentage survival relative to control cells. Data represent mean ± SD of three independent experiments. The impact of Alg-PVPI films on cell morphology was also monitored using a LEICA DMI6000B inverted microscope (Leica Microsystems, Wetzlar, Germany).

2.7. Wound Scratch Assay

HaCat were seeded into 24-well plates at 30×10^4 cells and were maintained at 37 °C and 5% CO_2 for 24 h to permit cell adhesion and the formation of a confluent monolayer. Subsequently, they were wounded with a sterile plastic pipette tip to leave a scratch of ≈0.4 mm in width. The cells were washed twice with PBS, and an Alg-PVPI film extract replaced the medium. Alg-PVPI film extracts were tested at the concentrations of 1, 2.5, and 5 mg mL^{-1}. All scratch assays were performed in triplicate. Wound closure was monitored, collecting digitized images immediately after scratching, 24 and 48 h post-induction. Images were analyzed using ImageJ software (National Institutes of Health, USA). Data have been reported as the extent of wound closure in the function of the initial scratch width.

2.8. Hemocompatibility

Hemocompatibility tests were performed to determine the blood compatibility of the proposed films for wound treatment, according to the ISO 10993-4 norm and standard practices for evaluating the interaction of a medical device or a material with blood.[19]

C57BL/6 mice ($n = 2$) weighing 23−24 g were used to draw blood. All procedures were performed following the Ethical Guidelines of the European Communities Council (Directive 2010/63/EU of 22 September 2010) and accepted by the Italian Ministry of Health. According to the "3Rs concept," every attempt was made to reduce animal suffering and to utilize the fewest number of animals necessary to provide accurate findings. Healthy mouse blood containing heparin (5000 U mL^{-1}) was taken and diluted with normal saline (4:5 ratio by volume). Fresh heparinized blood was stored at room temperature and used within 2 h of collection.

2.8.1. Hemolysis Assay

For the hemolysis test, samples with a 1.5×1.5 cm^2 exposure area were soaked in 2 mL normal physiological saline in 6-well culture plates and kept at 37 °C for 30 min. Normal physiological saline and distilled water served as negative and positive controls. After that, 0.04 mL diluted blood was added into each well and kept at 37 °C for another 60 min. Subsequently, the solutions were withdrawn and centrifuged at 3000 rpm for 10 min at room temperature. An aliquot of the supernatant (≈100 µL) was carefully removed and transferred to a 96-well plate for spectroscopic analysis using a Spark Multimode microplate reader (Tecan Group Ltd., Männedorf, Switzerland), and the absorbance (abs) was measured at 542 nm. The hemolysis rate was calculated according to Equation (1).

$$\text{Hemolysis Rate (\%)} = \frac{\text{sample abs} - \text{negative control abs}}{\text{positive control abs} - \text{negative control abs}} \times 100 \tag{1}$$

2.8.2. Blood Clotting Test

Blood clotting measurements were carried out to evaluate the hemostasis ability of the prepared films compared to commercial medical gauzes (Master-Aid Forte Med plasters, Pietrasanta Pharma, Italy). All the samples (1.5×1.5 cm) were placed into wells of 6-well plates and pre-warmed to 37 °C. Afterward, blood (100 µL) was added into each well, followed by $CaCl_2$ solution (0.1 м, 20 µL) to start the coagulation process. The samples were incubated at 37 °C for 5, 15, 30, and 60 min. Afterward, 5 mL of deionized water was carefully added to the wells along the inside wall. Hemolysis occurred to red blood cells that were not trapped in the stable clot. After 5 min, the supernatants were transferred into a 96-well plate, and a microplate reader measured the absorbance of samples at 542 nm. The blood clotting index (BCI) of the samples at each time point can be calculated by Equation (2):

$$\text{BCI (\%)} = \frac{I_s}{I_w} \times 100 \tag{2}$$

where I_s is the absorbance of blood that had contact with the sample, and I_w is the absorbance of blood hemolyzed with 5 mL of deionized water.

2.8.3. Blood Cells Adhesion Test

A 200 μL blood drop was placed on the samples (1.5 × 1.5 cm exposure area) and incubated for 30 min at 37 °C. Samples were then withdrawn, quickly rinsed three times with PBS to remove the non-specifically adsorbed cells, and then fixed with a 2% glutaraldehyde solution (pH 7.4 buffered with sodium cacodylate 0.1 M) at room temperature for 90 min. The fixative solution was then withdrawn, and the samples were washed three times for 10 min each with sodium cacodylate 0.1 M and stored overnight at 4 °C. Samples were post-fixed in 1% osmium tetroxide in the same buffer and then dehydrated in a graded ethanol series. Samples were sputter coated with 15 nm gold, and SEM analysis was performed as described in paragraph 2.3 to investigate blood cell adhesion and morphology.

2.9. Animal Models

2.9.1. Animals Storing

In vivo experiments were performed following the guidelines established by the European Communities Council Directive (Directive 2010/63/EU of 22 September 2010) and approved by the National Council on Animal Care of the Italian Ministry of Health, Number protocol 224/2020-PR, 5 March 2020. 8-12-week-old male CD1 and C57BL/6J mice were utilized. As described before for the hemocompatibility test (Section 2.8), also in this case, the 3Rs were followed for the in vivo tests. Mice were kept under a 12-h light/dark cycle (lights on at 8:00 am), relative humidity of (55 ± 10%), and at a controlled temperature of (21 ± 1 °C).

2.9.2. Hemorrhagic Test

CD1 mice of 25–30 g were randomly divided into two groups with five mice in each group, a control group and a group treated with Alg-PVPI films. The mice were anesthetized with a mixture of ketamine (10%) and xylazine (5%). The hemorrhagic test was performed as described in ref. [20]. Briefly, the liver was exposed via an anterior right subcostal incision. Behind the left lateral lobe, a pre-weighted cotton gauze (W_0) was gently placed. A 1 cm incision was induced by using a scalpel to mimic the hemorrhage process. Immediately after, the Alg-PVPI film was applied on the damaged area and the lack of bleeding for 5 min was considered as hemostasis. Finally, the gauzes were gently removed and weighed again (W_t) for measuring the blood loss utilizing Equation (3):

$$\text{Blood loss} = W_t - W_0 \tag{3}$$

During the experiment, the hemostatic time was also monitored.

2.9.3. Model of Diabetic Mice

C57BL/6J mice of 20–25 g were injected with 50 mg kg^{-1}, intraperitoneal, Streptozotocin (STZ, Merck Life Science, Milan,

Italy), dissolved in citrate buffer (sodium citrate, pH 4.5). The use of Streptozotocin is a widely diffused model for inducing diabetes. Indeed, Streptozotocin (STZ) is an antibiotic that, when administered to C57B6/J mice, causes the destruction of pancreatic β-cells and is used experimentally to produce a model of type 1 diabetes mellitus (T1DM).[21] Animals fasted for 4 h before STZ induction. The STZ-Na Citrate buffer solution was prepared immediately before injection due to the fast degradation of the drug in the Na-Citrate buffer after 15–20 min. Each mouse was treated with five consecutive intraperitoneal daily injections of STZ. Mice were tested to check levels of hyperglycemia at 4 weeks post-injection by drawing blood from the dorsal vein of the mouse. Animals with blood glucose levels of ±250 mg dL^{-1} were considered diabetic and used for the experiments.
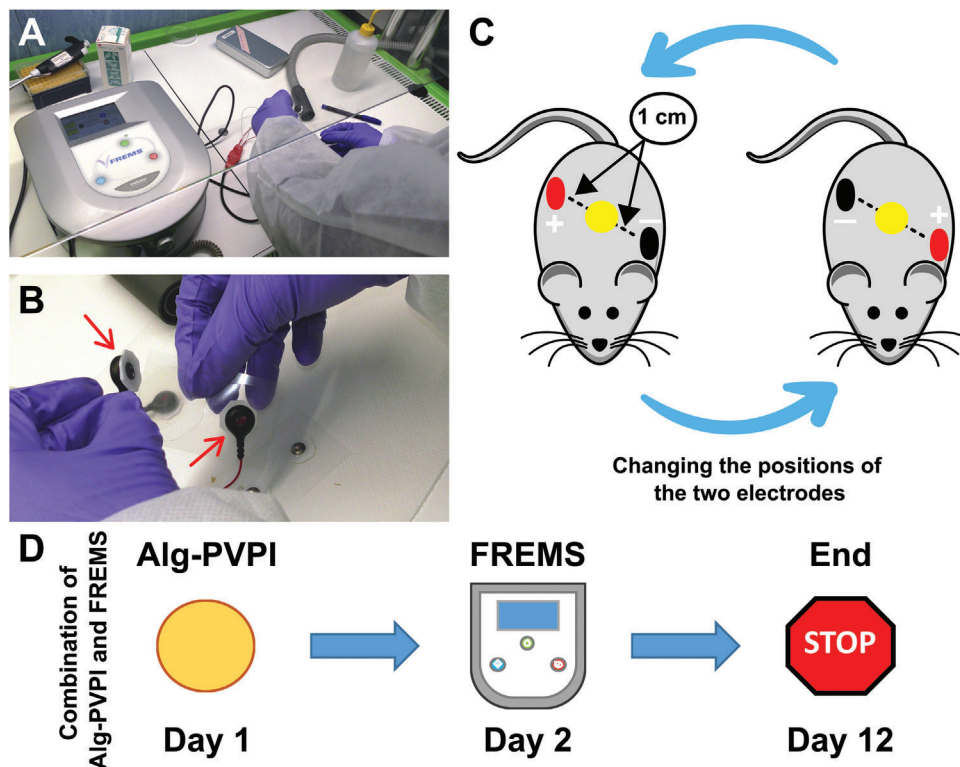
2.9.4. Wound Tests

To evaluate the wound closure, C57BL/6J diabetic mice were assigned to four groups with five mice for each group. The different groups were mice with no treated wounds (CTRL), treated with Alg-PVPI films, treated with FREMS, and treated with FREMS and Alg-PVPI films. The mice were anesthetized, their dorsal surface was shaved, and a full-thickness excisional wound was induced (diameter 6 mm). A photo of the wound was taken immediately after the biopsy generation (day 1). The bilayer dressing was applied, and pictures at days 1, 3, 5, 7, 9, and 12 were collected and analyzed using ImageJ software to quantify the wound closure rate. The wound closure was calculated as a percentage based on wound size relative to the control group. During the experiments, mice were housed individually and fed with water and food ad libitum.

2.9.5. Cytokines

C57BL/6J diabetic mice were assigned to five groups with five mice for each group (naïve, SHAM, treated with Alg-PVPI films, treated with FREMS, and treated with FREMS and Alg-PVPI films). The mice were anesthetized, their dorsal surface was shaved, and a full-thickness excisional wound was induced (diameter 6 mm). Skin samples from the five groups were collected on day 5, post-wound induction, and snap-frozen in liquid nitrogen. Cytokines (IL-6, IL-1β, and TNF-α) expression was measured using an ELISA quantikine kit (R & D system, Minneapolis, MN, USA), according to the manufacturer's instructions.[21b]

2.9.6. FREMS and Combined Application with Alg-PVPI Films

FREMS is a proprietary and patented technology of FREMLIFE (www.fremslife.com), which concerns the generation of biocompatible electrical signals by means of computerized neurostimulators and their administration through transcutaneous electrodes. FREMS is constituted by trains of sequences of electric pulses, characterized by a minimal quantity of charge, whose frequency and duration can be varied according to pre-set regimens. The amplitude of the impulse is set by the operator using a remote control, according to the patient's sensitivity threshold and the tissue stimulated. Subsequently, the system modulates maxi-

**ADVANCED
SCIENCE NEWS**

www.advancedsciencenews.com

{M}acro-
molecular

Bioscience

www.mbs-journal.de

Figure 1. FREMS technology and its application. A,B) Photographs of the spider system and the adhesive electrodes. C) Scheme of application of the electrodes on the mice wound models. The yellow circle is the wound, while the red and black spots represent the positive and negative electrodes, respectively. D) Application of the Alg-PVPI and FREMS for the in vivo tests: day 1 application of Alg-PVPI film; from day 2 FREMS treatment until day 12 (end of the experiment).

mum amplitude according to the ion balance of the tissue underneath the electrodes, to keep it constantly balanced (Biofeedback). Impulses have an active phase and a recovery phase, which guarantees the ion balance in the tissue involved in the process (see Figure S1, Supporting Information).

The impulse sequences are developed to suit the characteristics of the tissues to be involved in the programmed action, and they can activate a functional "recovery" mechanism in the area involved in the treatment (see Figure S1, Supporting Information). More than 100 different FREMS protocols are already clinically available to treat musculoskeletal disorders, sports injuries (muscle injuries, tendinopathies, etc.), peripheral neurovascular complications such as painful diabetic neuropathy, vasculopathies (arteriopathies, venous, or mixed stasis), and chronic ulcers of various etiologies.

The device used in this study is a portable apparatus commercially called SPEEDER, and the skin electrodes were cut to fit the small size of the mice, without modifying the electrical contact between the electrode and the skin (see **Figure 1**A,B).

The stimulation protocol used was that of traumatic ulcers applied for 30 mins and limited to 15 V (5% of maximum voltage) once a day, starting on day 2 and ending on day 12 of the experiment.
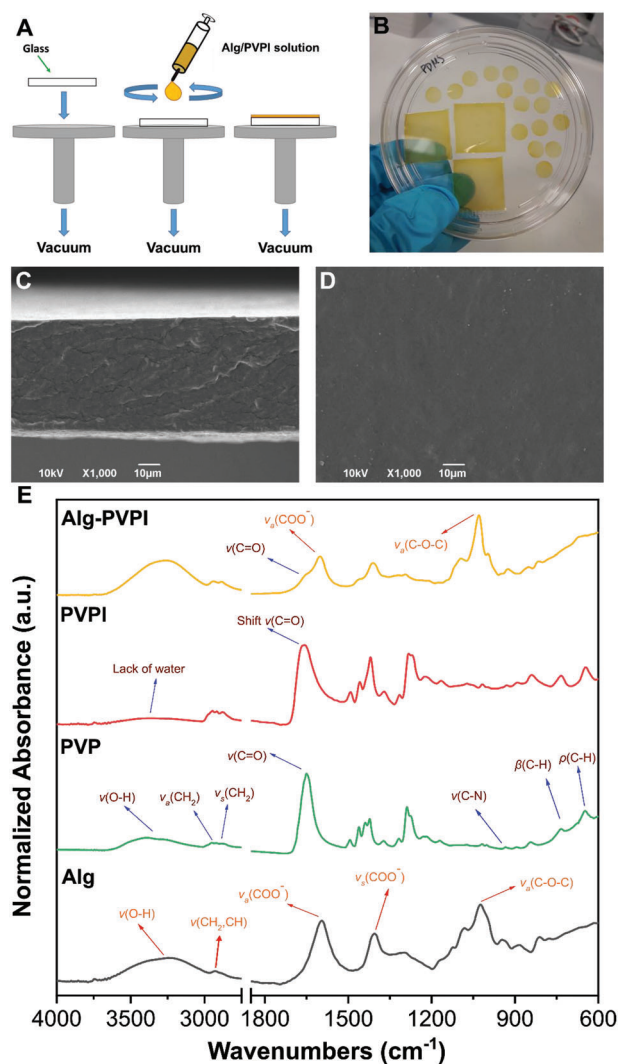
FREMS was applied on the shaved back of the mice by using hydrogel-based adhesive electrodes (see Figure 1A,B). The two adhesive electrodes were placed about 1 cm from the induced

wound (circular with a diameter of 0.6 cm), as schematically described in Figure 1C. The positive and negative electrodes were inverted daily to provide a unidirectional electric field-induced wound closure.

In the wound closure in vivo evaluation, Alg-PVPI films were applied immediately after the wound formation (day 1), while the FREMS treatment was added from the day after (day 2) until day 12 (Figure 1D). For the quantification of the cytokine expression, the test was stopped on day 5. In both experiments, FREMS treatment started on day 2 because the fresh wound (day 1) was unstable, and the weight of the adhesive electrodes altered the size and shape of the wound. Instead, on day 2, a protective scab was already present on the wounds, producing a natural layer that ensured not to modify the wound in the presence of the adhesive electrodes.

2.10. Statistics

For the statistical analysis of the proposed experiments, ANOVA was utilized to evaluate statistical significance, followed by Bonferroni's post-hoc test. The only exception was for the hemorrhagic tests were a t-test was used for performing the statistical analysis. GraphPad Prism 5 was used for all statistical analysis (GraphPad Software Inc., San Diego, CA, USA). Results with a p-value < 0.05 were considered statistically significant.

**ADVANCED
SCIENCE NEWS**

www.advancedsciencenews.com

[M] acro-
olecular

Bioscience

www.mbs-journal.de

Figure 2. Preparation and characterization of Alg-PVPI films. A) Scheme of fabrication of the Alg-PVPI-based samples using a spin coater. B) Photograph of the produced biomaterials. CD) SEM images of Alg-PVPI top view and cross-section, respectively. E) ATR-FTIR spectra of Alg-PVPI, PVPI, PVP, and Alg.

3. Results and Discussion

3.1. Film Characterization

Alg-PVPI films were fabricated using a spin coater as schematically described in **Figure 2**A. The obtained films had an orange color and a thickness of $80 \pm 10 \, \mu m$ (see Figure 2B). Characteristic SEM images of the top-view and cross-section for the Alg-PVPI films are shown in Figure 2C,D, respectively. The films' surfaces and cross-sections were smooth, and no phase separation was observed, indicating that the ingredients were well-blended.

Similar Alg-PVPI films developed by Liakos et al. had shown phase separation.[12a] The authors had used the solvent casting method to produce those films, with Alginate and PVPI having more time during the evaporation of the solvents to phase sep-

arate. Hence, the spin coating technique, used in this work, ensures a better and more homogenous mixing during the fabrication of the samples.
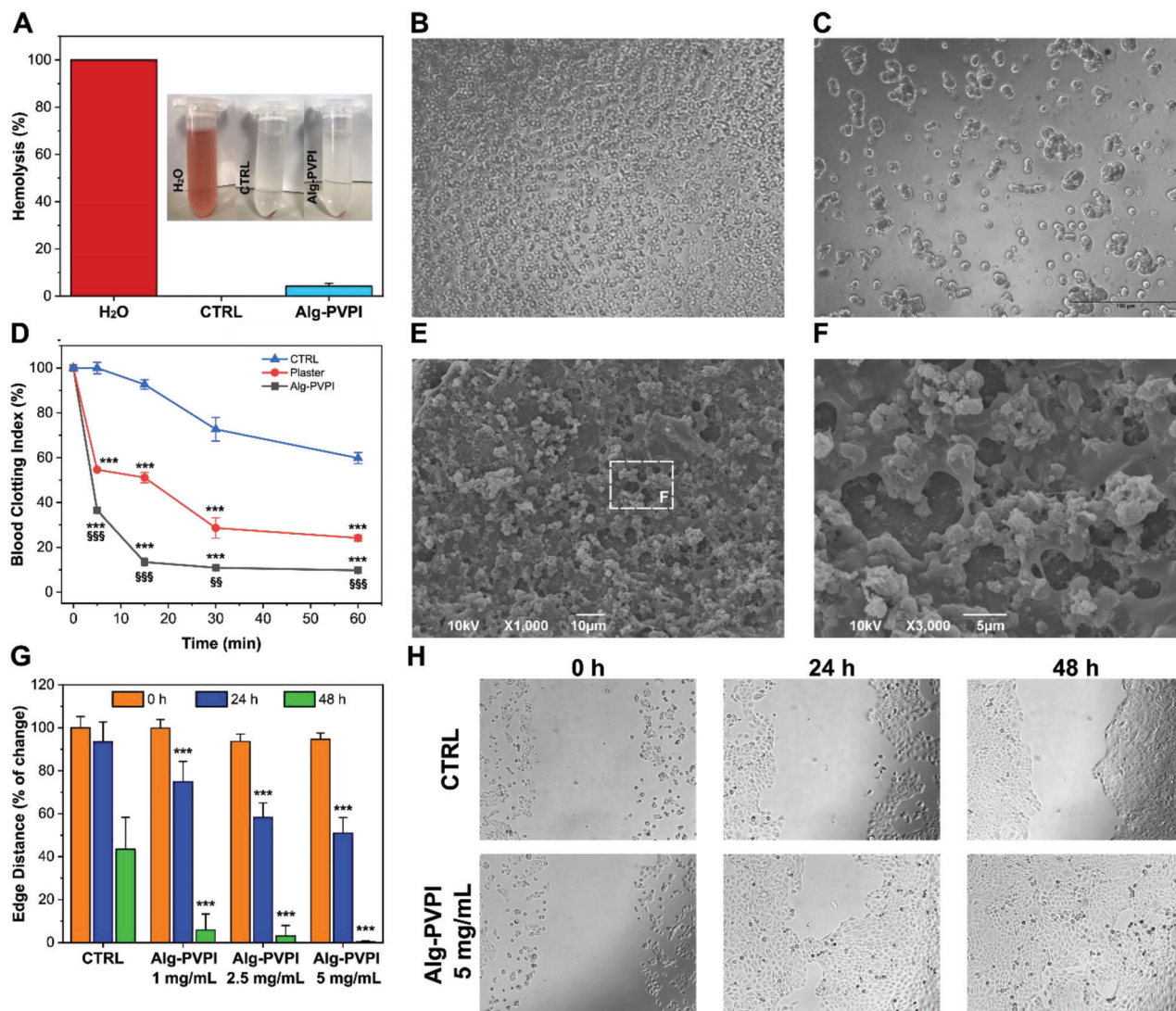
ATR-FTIR spectra of Alg, PVP, PVPI, and Alg-PVPI are reported in Figure 2D. Alg showed typical peaks of O–H stretching modes at 3383 and 3212 cm^{-1}, asymmetric and symmetric CH$_2$ and CH stretching modes at 2937, 2917, 2889, and 2860 cm^{-1}, asymmetric and symmetric COO$^-$ stretching modes at 1595 and 1406 cm^{-1}, symmetric C–O–C stretching mode at 1024 cm^{-1}. In the PVP spectrum, the following vibration modes were observed: O–H stretching mode at 3408 cm^{-1}, asymmetric and symmetric CH$_2$ stretching modes at 2982, 2948, 2918, and 2874 cm^{-1}, respectively, C = O stretching mode at 1650 cm^{-1}, C–N stretching mode at 1018 cm^{-1}, out-of-plane C–H bending mode at 841 cm^{-1}, and C–H rocking mode at 733 cm^{-1}. These peaks are mostly connected with the chemical structure of PVP.[22] In the PVPI spectrum, all the main vibrations are referred to the PVP structure. However, a shift of the C = O stretching mode to 1660 cm^{-1} was found. This shift relates to the interaction between the amide group of PVP with the iodine. In the Alg-PVPI spectrum, the overlapped peaks of the two polymers are present, and the vibration modes attributed to PVPI and Alg are highlighted in the graph by the blue and red arrows, respectively. However, a shift and a different shape of the C–O–C stretching mode of Alg were noticed due to the overlapping presence of the C–O stretching mode of the Gly present in Alg-PVPI films.

The average value of WCA of Alg-PVPI was 39.5 ± 1.2 (Figure S2, Supporting Information), which demonstrates the highly hydrophilic nature of the alginate-based films, as previously reported. The hydrophilicity is an essential property for wound dressings, in order to absorb exudate and release the antiseptic molecules.[23]

3.2. In Vitro Biocompatibility, Hemocompatibility, and Clotting Properties

Biocompatibility is the first requirement for every biomaterial that should be placed in contact with the fluids and the tissues of our body. For this reason, Alg-PVPI film extracts at different concentrations were tested on keratinocytes, one of the main cell types that compose the skin tissue. The results are shown in Figure S3 (Supporting Information). The Alg-PVPI films resulted in being fully biocompatible, and no toxic effects were detected for all the concentrations tested.

Hemocompatibility is one of the leading requirements in directing the design of innovative patches, films, and blood-contacting materials in general. An ideal material for wound treatments should provoke low hemolysis and favorable coagulation kinetics. In particular, the films should present a hemolysis value of less than 5% to be suitable for skin tissue regeneration, a limit set by the ISO 10993-4 standard. Alg-PVPI films demonstrated high hemocompatibility with a hemolysis percentage of $3.8 \pm 0.9\%$ (**Figure 3**A) after being in contact with blood for 60 min. These results were also confirmed by the optical microscope investigation (Figure 3B,C), and they align with the available data in the literature regarding the hemolysis rate of alginate-based and PVPI-based wound dressings.[13b,24]

**ADVANCED
SCIENCE NEWS**

www.advancedsciencenews.com

[M]acro-
molecular

Bioscience

www.mbs-journal.de

Figure 3. In vitro analysis. A) Histogram relative to the absorbance of released hemoglobin after treatment with H_2O (MilliQ), CTRL (saline solution), and Alg-PVPI. Results are presented as the average ± SD ($n = 3$). BC) Optical images of blood after the treatment with CTRL (saline solution) and Alg-PVPI, respectively. D) Blood clotting index for CTRL (saline solution), Plaster, and Alg-PVPI. ***$p < 0.001$ versus CTRL; §§$p < 0.01$ versus Plaster; §§§$p < 0.001$ versus Plaster. Results are presented as the average ± SD ($n = 3$). EF) SEM images of a blood clot on Alg-PVPI surface at two different magnifications. G) Quantification of the edge distance in the wound scratch test at 0, 24, and 48 h. ***$p < 0.001$ versus CTRL. Results are presented as the average ± SD ($n = 5$). H) Optical images of wound scratch experiment for CTRL and Alg-PVPI 5 mg mL^{-1} after 0, 24, and 48 h.

An ideal wound dressing should also promote platelets and red blood cells (RBCs) to aggregate at the wound site and form a blood clot to accelerate the hemostasis.[25] The BCI is an effective quantitative index to evaluate the coagulation performance of different materials, and it is calculated from the absorbance (at 542 nm) of free hemoglobin not involved in the coagulation process. The blood-clotting index of the prepared dressing was calculated and compared with a commercially available plaster. The results are represented in Figure 3D, with a lower BCI indicating higher blood-clotting efficiency. In this study, a significant difference was noticed between the Alg-PVPI samples and both the plaster and control samples after being incubated with whole blood for 5, 15, 30, and 60 min. This may be due to the synergistic effect of alginate and PVPI on hemostasis.[26] The results

were supported by erythrocyte microscopy analysis (Figure 3C), where it can be noticed that Alg-PVPI films induce the agglutination of erythrocytes, whose membranes result intact (i.e., non-hemolyzed).

Figure 3E,F and Figure S4 (Supporting Information) show the adhesion and morphology of red blood cells and platelets on the Alg-PVPI sample surface. The platelets adhering to the films were aggregated and had round morphology with a few filopodia. These results indicated that platelets could be effectively attached to the surface of Alg-PVPI samples and play a role in the hemostatic process.

In the wound healing process, the further step is cell proliferation after the initial stages of hemostasis and inflammation. A wound scratch test was performed to evaluate the capacity of Alg-
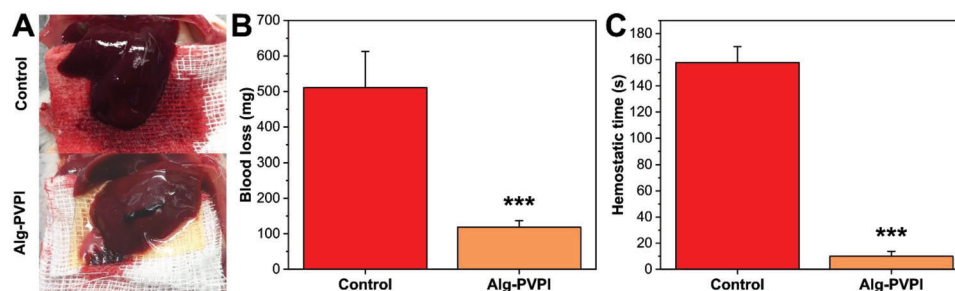
Figure 4. Hemorrhagic test. A) Photographs of control and Alg-PVPI film-treated livers after 5 min from the cut. BC) Results of the blood loss and hemostatic time, respectively, for the control and Alg-PVPI groups. Results are presented as the average ± SD. ***$p < 0.001$ versus CTRL ($n = 5$ for each group).

PVPI films to induce cell growth, and the results are displayed in Figure 3G,H. The keratinocytes treated with Alg-PVPI films had a statistically higher proliferation speed after 24 and 48 h with respect to the control. Indeed, the treated keratinocytes completed the closing of the wound scratch in 48 h, while in the untreated cells, 40% of the wound edge was not healed during the same period.

Altogether, these outcomes highlighted that Alg-PVPI films have a high level of bio- and hemocompatibility, a clotting effect, and the capacity to promote cell proliferation, confirming to be an excellent candidate for application in acute and chronic wounds and for supporting their healing.

3.3. Hemorrhagic Test

Hemostasis is the first step for wound healing to start and, in emergency cases, is a vital process to occur after an injury.[6a,9] Considering the excellent clotting properties of the Alg-PVPI film shown in the in vitro analysis, a hemorrhagic test was performed in mice. Photographs of the control and Alg-PVPI film-treated livers are displayed in **Figure 4**A. The blood loss and hemostatic time were calculated from the test, and the results are graphed in Figure 4B,C. The control sample released around 500 mg of blood, and the hemorrhage stopped after almost 3 min. On the other hand, applying the Alg-PVPI film on the injured liver, immediately interrupted the bleeding with a hemostatic time of a few seconds and a blood loss of around 100 mg. Together with the previous results, these findings confirmed the excellent properties of Alg-PVPI films in the interaction with blood without causing any toxic effects, inducing hemostasis and clotting. Thus, Alg-PVPI films have extraordinary potential for wound healing applications.

3.4. Wound Closure and Anti-Inflammatory Properties in In Vivo Diabetic Mice Models

The effect of the combination of FREMS technology with Alg-PVPI films was evaluated in the diabetic mice model. Firstly, the wound closure rate was investigated, and the main results are reported in **Figure 5**A,B. As can be noticed, during the monitoring period (12 days), the wounds of the non-treated mice (CTRL) did not heal due to the diabetic condition, showing that 80% of the wound area was still unrecovered. The application of FREMS technology showed a gradual wound closure and led to a recovery of 70% of the initial damaged wound area. FREMS technology was statistically better than the controls (see Figure 5B). The mice treated with PVPI-based patches showed a slight difference in the progression of the wound-healing process. Indeed, an initial stronger effect of the closure process, both with respect to the controls and the FREMS technology, has been observed until the first 7 days. After 12 days, the mice treated with PVPI-based patches showed a residual wound area of 23%, which was statistically better than the CTRL and similar to the FREMS group.

Finally, the mice treated both with the wound dressing and the FREMS technology showed an ameliorated progression of wound healing rate. Indeed, from the first days, the wound condition was statistically improved both concerning the CTRL and the FREMS, mimicking the outcome of the PVPI-based patch tested alone. Interestingly, after 5 days, the enhancement in the wound repair resulted in being statistically better than in the mice treated with the PVPI-based patch. In the end, after 12 days, the mice treated with the two technologies showed complete recovery of wounds, while the control recovered only the 20% of the initial wound area, the FREMS group the 70%, and the Alg-PVPI group the 73%.

According to these data, Alg-PVPI and FREMS alone could accelerate but not complete wound closure. Instead, the combination of Alg-PVPI and FREMS technology was able to close the induced wound in 12 days, suggesting a positive synergic effect of the two technologies.

Alterations in the blood flow and the persistence of inflammatory conditions are the main reasons for unsolved diabetic ulcers. Therefore, measuring the level of inflammatory mediators after applying the two technologies is a crucial point to be evaluated.

The main results on the inflammatory mediators' levels after 5 days from the induced wound damage in the in vivo diabetic mice model are reported in **Figure 6**A–C. The levels of TNF-α (see Figure 6A) were higher in the SHAM mice, while the values in the mice treated with FREMS, Alg-PVPI, and FREMS/Alg-PVPI were statistically lower. Moreover, the values of TNF-α found in the mice treated with PVPI and FREMS/Alg-PVPI were also statistically lower than FREMS. The IL-6 levels for the FREMS, PVPI, and FREMS/Alg-PVPI groups were statically reduced with respect to the SHAM mice. However, in this case, FREMS/Alg-PVPI treatment produced the lowest levels of IL-6, being statistically lower even than FREMS and PVPI alone (see
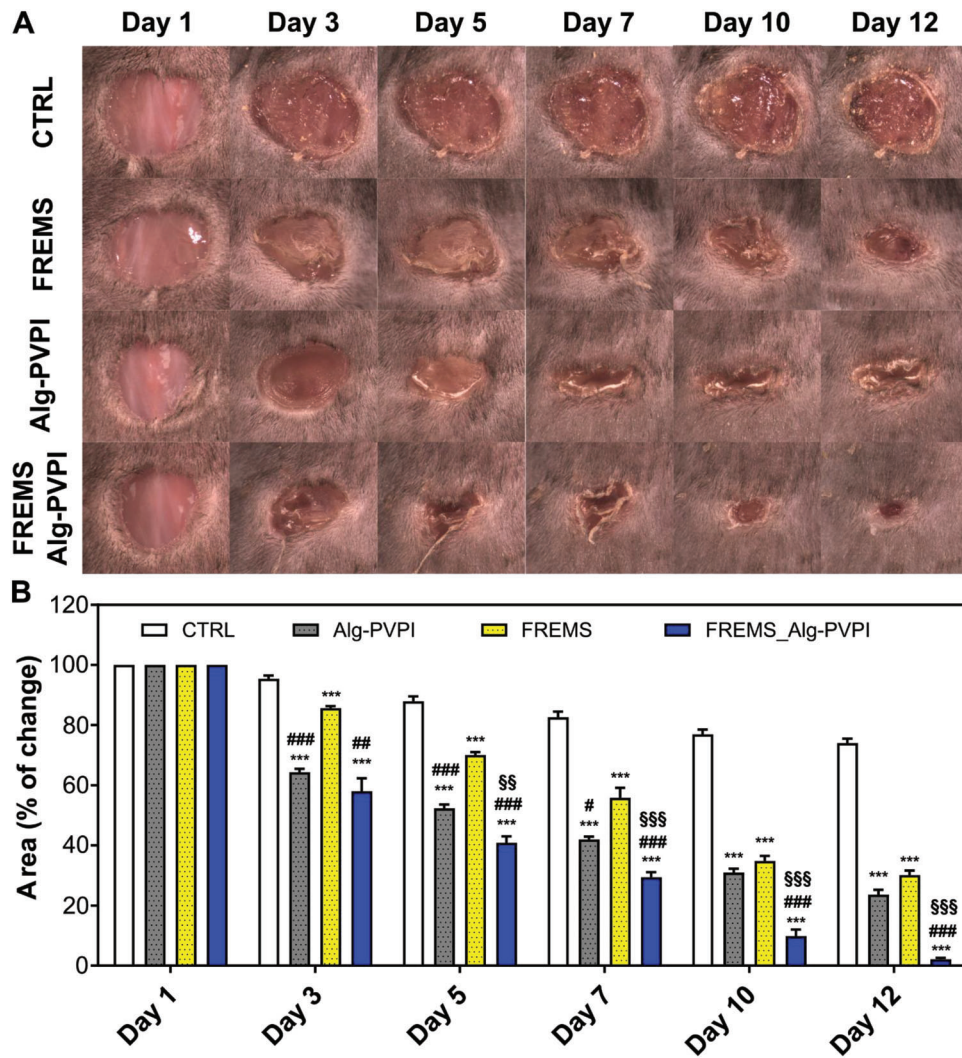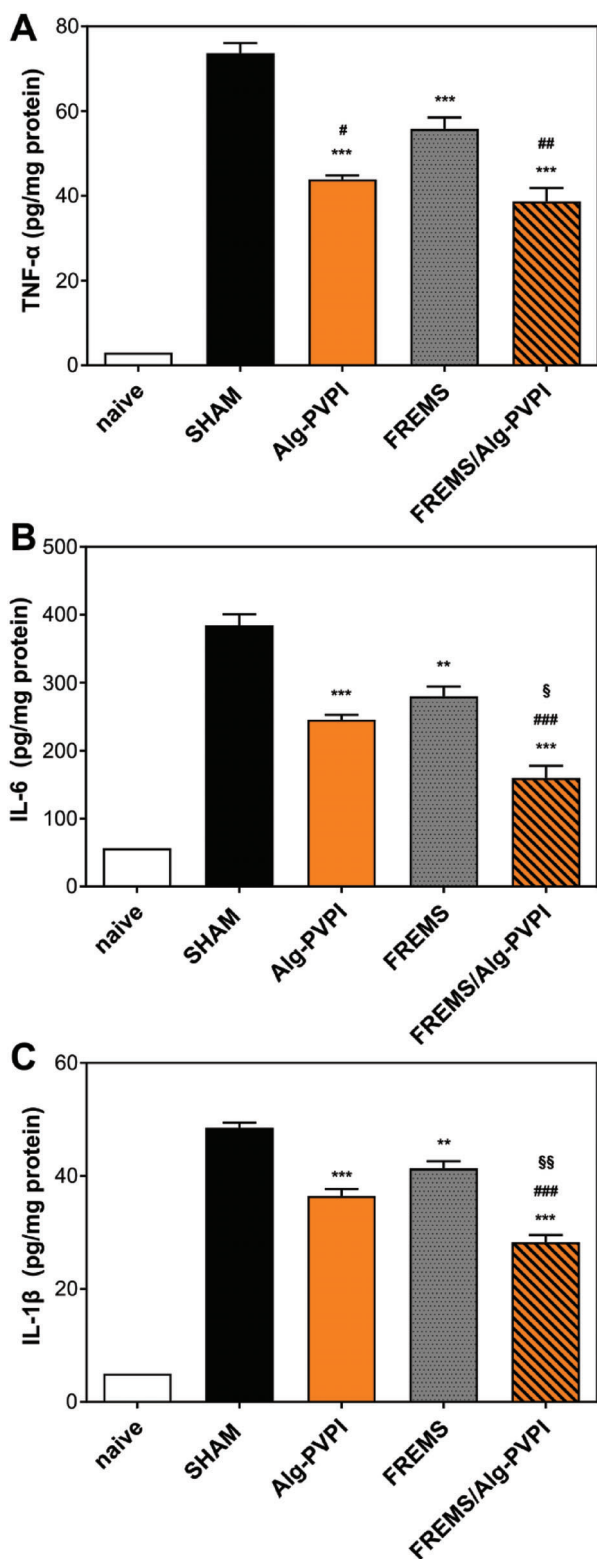
Figure 5. In vivo wound closure rate. A) Photographs of diabetic wound no treated (CTRL), treated with FREMS technology (FREMS), with Alg-PVPI-based patch (Alg-PVPI), and with the combination of FREMS technology and Alg-PVPI-based patch (FREMS/Alg-PVPI). B) Quantification of wound area closure for CTRL, FREMS, Alg-PVPI, and FREMS/Alg-PVPI. Results are presented as the average ± SD. ***$p < 0.001$ versus CTRL; #$p < 0.05$ versus FREMS; ##$p < 0.01$ versus FREMS; ###$p < 0.001$ versus FREMS; §§$p < 0.01$ versus Alg-PVPI; §§§$p < 0.001$ versus Alg-PVPI ($n = 5$ each group).

Figure 6B). A similar trend was also observed for the quantities of IL-1β in the FREMS/Alg-PVPI group, showing that this group was most performing in reducing this inflammatory mediator's level (Figure 6C).

Hence, the in vivo analysis outcomes highlighted a different progression in the wound closure rate. FREMS has a more gradual effect connected with its daily application and capacity to increase blood flow and to recall pro-healing factors such as VEGF. Alg-PVPI had a more substantial impact in the first days, immediately after its application, and a slower progression toward final healing. Both FREMS and Alg-PVPI statistically reduced the investigated inflammatory mediators suggesting another aspect to consider in explaining their effect with respect to the control.

The most important finding was the synergism in the effect of FREMS and Alg-PVPI in wound healing and the reduction of inflammation. The hypothetical reason for this effect can be sought into the presence of the alginate-based dressing which absorbs moisture from the wound bed, keeping the wound environment in a suitable wet condition.[11b] Also, alginate has been proven to enhance the proliferation of skin cells such as fibroblast and keratinocytes, as also shown in this work.[23c] Moreover, the presence of the antimicrobial agent PVPI inside the dressing reduces the probability of infection during the healing process, and thus, it can prove this latter. The combination of all these effects mediated by the Alg-PVPI dressing, along with the aforementioned proliferative and accelerating benefits led by the FREMSTM, can potentially ameliorate the rate of wound healing phases (hemostasis, inflammation, proliferation, and remodeling) and explain why we observed this synergism in our study. The observed synergism can be a perfect match to enhance the current performance of electrical stimulation-based technologies for treating complex wounds in patients with diabetes. These preliminary results are obtained from tests in a mouse model, which is far from an actual diabetic ulcer in a

ADVANCED
SCIENCE NEWS
www.advancedsciencenews.com

[M]acro-molecular
Bioscience
www.mbs-journal.de

Figure 6. Anti-inflammatory properties. A–C) Levels of TNF-α, IL-6, and IL-1β of naive, SHAM, Alg-PVPI, FREMS, FREMS/Alg-PVPI groups. Results are presented as the average ± SD. **$p < 0.01$ versus SHAM; ***$p < 0.001$ versus SHAM; #$p < 0.05$ versus FREMS; ##$p < 0.01$ versus FREMS; ###$p < 0.001$ versus FREMS; §$p < 0.05$ versus Alg-PVPI; §§$p < 0.01$ versus Alg-PVPI; §§§$p < 0.001$ versus Alg-PVPI ($n = 5$ each group).

human being. However, FREMS technology has already been tested clinically on diabetic patients and has shown several positive effects. For humans, the protocolled treatment is based on applying FREMS for treatment lasting up to 60 days (in case of diabetic ulcers)[18a-d]. Ideally, Alg-based film dressing could be used daily or along the treatment to block potential infections, enhance the proliferation of keratinocytes, absorb exudate, and accelerate the final possible success of the synergic therapy.

This new strategy can potentially reduce the morbidity rates due to its showed positive effect on the wound healing. Meanwhile, since both FREMS technology and the wound patch can easily be used at home by the patients, this therapy can impact on the cost and the life quality of the patient which would not need to go anymore to the hospital or equipped centers for their daily therapy and would not need potentially any other further assistance from nursery in this regard.

4. Conclusions

The management of difficult skin ulcerative lesions, both in terms of direct and indirect costs, represents a huge cost for the National Health System. In fact, in Italy about 2 million individuals are affected by this pathology, which also indirectly affects their families. The problem is more relevant for patients assisted at home, and it is a problem destined to grow in the future both from an organizational and economic point of view. In this work, we present an efficient solution to this problem, combining FREMS technology with an alginate-based wound dressing to treat chronic diabetic ulcers.

The dressing films were fabricated by spin coating, resulting in a good blend between alginate and the active component PVP-I. The bioactive films were hydrophilic and with a high degree of biocompatibility. In vitro tests showed how the films can promote keratinocyte migration and proliferation in a wound scratch model, have excellent hemocompatibility, and, simultaneously, good clotting properties. Next, the developed Alg/PVP-I-based films were tested in combination with FREMS in diabetic mice models. The outcome was a significant enhancement in the closure of chronic wounds due to the combination of the two medical devices. Moreover, the levels of inflammatory mediators, such as IL-6, IL-1β, and TNF-α, were reduced in the mice treated with FREMS and Alg-PVPI. The overall results demonstrate how the simultaneous application of FREMS technology and the bioactive wound dressing can enhance the capacity of both devices to treat difficult-to-heal wounds in patients with diabetes, opening new perspectives not only in terms of research but also at the hospital level in a real scenario, and highlighting the possibility to have an impact in reshaping and ameliorating standard clinical practices. This work paves the way to new therapeutic methodologies that combine neurostimulation with the use of advanced biomaterials, which can greatly contribute, maybe combined with the advancement in AI and OMICS,[27] to improving the quality of life of diabetic patients with skin ulcerative lesions and reducing the social costs of these pathologies.

Supporting Information

Supporting Information is available from the Wiley Online Library or from the author.

Conflict of Interest

The authors declare no conflict of interest.

Data Availability Statement

The data that support the findings of this study are available from the corresponding author upon reasonable request.

Keywords

[1] J. M. P. Holly, K. Biernacka, N. Maskell, C. M. Perks, *Front. Endocrinol.* **2020**, *11*, 582870.

[2] W. H. Organization, Geneva: World Health Organization **2016**.

[3] a) S. Paul, A. Ali, R. Katare, *J. Diabetes Its Complications* **2020**, *34*, 107613; b) P. Picone, S. Vilasi, F. Librizzi, M. Contardi, D. Nuzzo, L. Caruana, S. Baldassano, A. Amato, F. Mulè, P. L. San Biagio, D. Giacomazza, M. Di Carlo, *Aging(Albany, NY)* **2016**, *8*, 1718.

[4] a) L. Martinengo, M. Olsson, R. Bajpai, M. Soljak, Z. Upton, A. Schmidtchen, J. Car, J. Järbrink, *Ann. Epidemiol.* **2019**, *29*, 8. b) T. M. Klein, V. Andrees, N. Kirsten, K. Protz, M. Augustin, C. Blome, *Int. Wound J.* **2021**, *18*, 287.

[5] F. Rancan, J. Jurisch, S. Hadam, A. Vogt, U. Blume-Peytavi, I. S. Bayer, M. Contardi, C. Schaudinn, *Pharmaceutics* **2023**, *15*, 1876.

[6] a) G. C. Gurtner, S. Werner, Y. Barrandon, M. T. Longaker, *Nature* **2008**, *453*, 314; b) D. Simões, S. P. Miguel, M. P. Ribeiro, P. Coutinho, A. G. Mendonça, I. J. Correia, *Eur. J. Pharm. Biopharm.* **2018**, *127*, 130; c) K. Singh, V. B. Yadav, U. Yadav, G. Nath, A. Srivastava, P. Zamboni, P. Kerkar, P. S. Saxena, A. V. Singh, *Colloids Surf., A* **2023**, *670*, 131575.

[7] M. Chang, T. T. Nguyen, *Acc. Chem. Res.* **2021**, *54*, 1080.

[8] a) M. Mirhaj, S. Labbaf, M. Tavakoli, A. Seifalian, *Macromol. Biosci.* **2022**, *22*, 2200014; b) M. Contardi, J. A. Heredia-Guerrero, S. Guzman-Puyol, M. Summa, J. J. Benítez, L. Goldoni, G. Caputo, G. Cusimano, P. Picone, M. Di Carlo, R. Bertorelli, A. Athanassiou, I. S. Bayer, *J. Mater. Chem. B* **2019**, *7*, 1384; c) M. Contardi, J. A. Heredia-Guerrero, G. Perotto, P. Valentini, P. P. Pompa, R. Spanò, S. Goldoni, R. Bertorelli, A. Athanassiou, I. S. Bayer, *Eur. J. Pharm. Sci.* **2017**, *104*, 133; d) M. Contardi, D. Kossyvaki, P. Picone, M. Summa, X. Guo, J. A. Heredia-Guerrero, D. Giacomazza, R. Carzino, L. Goldoni, G. Scoponi, F. Rancan, R. Bertorelli, M. Di Carlo, A. Athanassiou, I. S. Bayer, *Chem. Eng. J.* **2021**, *409*, 128144; e) M. Contardi, A. Alfaro-Pulido, P. Picone, S. Guzman-Puyol, L. Goldoni, J. J. Benítez, A. Heredia, M. J. Barthel, L. Ceseracciu, G. Cusimano, O. R. Brancato, M. Di Carlo, A. Athanassiou, J. A. Heredia-Guerrero, *PLoS One* **2019**, *14*, e0214956.

[9] M. Contardi, M. Lenzuni, F. Fiorentini, M. Summa, R. Bertorelli, G. Suarato, A. Athanassiou, *Pharmaceutics* **2021**, *13*, 999.

[10] a) G. D. Mogosanu, A. M. Grumezescu, *Int. J. Pharm.* **2014**, *463*, 127; b) M. E. Antinori, M. Contardi, G. Suarato, A. Armirotti, R. Bertorelli, G. Mancini, D. Debellis, A. Athanassiou, *Sci. Rep.* **2021**, *11*, 12630; c) M. Ruggeri, D. Miele, M. Contardi, B. Vigani, C. Boselli, A. I. Cornaglia, S. Rossi, G. Suarato, A. Athanassiou, G. Sandri, *Front. Bioeng. Biotechnol.* **2023**, *11*, 1225722.

[11] a) H. Hajiali, M. Summa, D. Russo, A. Armirotti, V. Brunetti, R. Bertorelli, A. Athanassiou, E. Mele, *J. Mater. Chem. B* **2016**, *4*, 1686; b) K. Varaprasad, T. Jayaramudu, V. Kanikireddy, C. Toro, E. R. Sadiku, *Carbohydr. Polym.* **2020**, *236*, 116025; c) A. Barbu, B. Neamtu, M. Zahan, G. M. Iancu, C. Bacila, V. Mire?An, *J. Pers. Med.* **2021**, *11*, 890.

[12] a) I. Liakos, L. Rizzello, I. S. Bayer, P. P. Pompa, R. Cingolani, A. Athanassiou, *Carbohydr. Polym.* **2013**, *92*, 176; b) M. Summa, D. Russo, I. Penna, N. Margaroli, I. S. Bayer, T. Bandiera, A. Athanassiou, R. Bertorelli, *Eur. J. Pharm. Biopharm.* **2018**, *122*, 17; c) P. L. Bigliardi, S. A. L. Alsagoff, H. Y. El-Kafrawi, J.-K. Pyon, C. T. C. Wa, M. A. Villa, *Int. J. Surg.* **2017**, *44*, 260.

[13] a) S. G. Priya, A. Gupta, E. Jain, J. Sarkar, A. Damania, P. R. Jagdale, B. P. Chaudhari, K. C. Gupta, A. Kumar, *ACS Appl. Mater. Interfaces* **2016**, *8*, 15145; b) S. M. Andrabi, P. Singh, S. Majumder, A. Kumar, *Chem. Eng. J.* **2021**, *423*, 130219; c) F. Rancan, M. Contardi, J. Jurisch, U. Blume-Peytavi, A. Vogt, I. S. Bayer, C. Schaudinn, *Pharmaceutics* **2019**, *11*, 527.

[14] N. Attal, D. Bouhassira, R. Baron, *Lancet Neurol.* **2018**, *17*, 456.

[15] D. Ziegler, *Diabetes/Metab. Res. Rev.* **2008**, *24*, S52.

[16] E. Bosi, G. Bax, L. Scionti, V. Spallone, S. Tesfaye, P. Valensi, D. Ziegler, *Diabetologia* **2013**, *56*, 467.

[17] a) E. Bosi, M. Conti, C. Vermigli, G. Cazzetta, E. Peretti, M. C. Cordoni, G. Galimberti, L. Scionti, *Diabetologia* **2005**, *48*, 817; b) A. Bandini, S. Orlandi, C. Manfredi, A. Evangelisti, M. Barrella, M. Bevilacqua, L. Bocchi, *Microvasc. Res.* **2013**, *88*, 42; c) D. Gorczyca-Siudak, P. Dziemidok, *Int. J. Environ. Res. Public Health* **2023**, *20*, 111.

[18] a) A. Jankovic, I. Binic, *Arch. Dermatol. Res.* **2008**, *300*, 377; b) A. Santamato, F. Panza, F. Fortunato, A. Portincasa, V. Frisardi, G. Cassatella, M. Valente, D. Seripa, M. Ranieri, P. Fiore, *Rejuvenation Res* **2012**, *15*, 281; c) S. O. Popa, M. Ferrari, G. M. Andreozzi, R. Martini, A. Bagno, *Med. Eng. Phys.* **2015**, *37*, 1111; d) C. Magnoni, E. Rossi, C. Fiorentini, A. Baggio, B. Ferrari, G. Alberto, *J. Wound Care* **2013**, *22*, 525; e) M. Bevilacqua, L. J. Dominguez, M. Barrella, M. Barbagallo, *J. Endocrinol. Invest.* **2007**, *30*, 944.

[19] M. Lenzuni, S. Bonfadini, L. Criante, F. Zorzi, M. Summa, R. Bertorelli, G. Suarato, A. Athanassiou, *Lab Chip* **2023**, *23*, 1576.

[20] R. Ding, X. Wei, Y. Liu, Y. Wang, Z. Xing, L. Wang, H. Liu, Y. Fan, *Smart Mater. Med.* **2023**, *4*, 173.

[21] a) M. L. Graham, J. L. Janecek, J. A. Kittredge, B. J. Hering, H.-J. Schuurman, *Comp. Med.* **2011**, *61*, 356; b) M. Contardi, M. Summa, P. Picone, O. R. Brancato, M. Di Carlo, R. Bertorelli, A. Athanassiou, *Pharmaceutics* **2022**, *14*, 483.

[22] M. Contardi, D. Russo, G. Suarato, J. A. Heredia-Guerrero, L. Ceseracciu, I. Penna, N. Margaroli, M. Summa, R. Spanò, G. Tassistro, L. Vezzulli, T. Bandiera, R. Bertorelli, A. Athanassiou, I. S. Bayer, *Chem. Eng. J.* **2019**, *358*, 912.

[23] a) M. Fadda, M. Contardi, S. Dante, M. Di Carlo, G. Galizzi, A. Athanassiou, I. S. Bayer, *Prog. Org. Coat.* **2022**, *168*, 106883; b) M. Lenzuni, G. Suarato, D. Miele, R. Carzino, M. Ruggeri, R. Bertorelli, G. Sandri, A. Athanassiou, *RSC Adv.* **2021**, *11*, 24345; c) M. Contardi, A. Md. Md. Ayyoub, M. Summa, D. Kossyvaki, M. Fadda, N. Liessi, A. Armirotti, D. Fragouli, R. Bertorelli, A. Athanassiou, *ACS Appl. Bio Mater.* **2022**, *5*, 2880.

[24] M. Zare-Gachi, H. Daemi, J. Mohammadi, P. Baei, F. Bazgir, S. Hosseini-Salekdeh, H. Baharvand, *Mater. Sci. Eng., C* **2020**, *107*, 110321.

[25] S. Pourshahrestani, E. Zeimaran, N. A. Kadri, N. Mutlu, A. R. Boccaccini, *Adv. Healthcare Mater.* **2020**, *9*, 2000905.

[26] a) H. Huang, H. Chen, X. Wang, F. Qiu, H. Liu, J. Lu, L. Tong, Y. Yang, X. Wang, H. Wu, *ACS Biomater. Sci. Eng.* **2019**, *5*, 5498; b) B. P. R. Kumar, A. Maddi, K. V. Ramesh, M. J. Baliga, S. N. Rao, Meenakshi, *Int. J. Oral Surg.* **2006**, *35*, 765.

[27] A. V. Singh, V. Chandrasekar, N. Paudel, P. Laux, A. Luch, D. Gemmati, V. Tissato, K. S. Prabhu, S. Uddin, S. P. Dakua, *Biomed. Pharmacother.* **2023**, *163*, 114784.